Supporting Information

Etching-Assisted Route to Heterophase Au Nanowires with Multiple Types of Active Surface Sites for Silane Oxidation

Chaoqi Wang,[†, ‡] *Xiang Li,*[†, §] *Lei Jin,*[//] *Peng-Han Lu,*[//] *Catherine Dejoie,*[⊥] *Wenxin Zhu,*[‡] *Zhenni Wang,*[†] *Wei Bi,*[†] *Rafal E. Dunin-Borkowski,*[//] *Kai Chen,*[‡,] * *and Mingshang Jin*[†,] *

[†] Frontier Institute of Science and Technology and State Key Laboratory for Mechanical Behavior of Materials, Xi'an Jiaotong University, Xi'an, Shaanxi 710049, China

[‡] Center for Advancing Materials Performance from the Nanoscale (CAMP-Nano), State Key Laboratory for Mechanical Behavior of Materials, Xi'an Jiaotong University, Xi'an, Shaanxi 710049, China

[§]Institute of Advanced Electrochemical Energy and School of Materials Science and Engineering, Xi'an University of Technology, Xi'an, Shaanxi 710048, China

[//] Ernst Ruska-Centre for Microscopy and Spectroscopy with Electrons and Peter Grünberg Institute, Forschungszentrum Jülich, 52425 Jülich, Germany.

[⊥] Structure of Materials Group, ESRF-The European Synchrotron CS40220, 38043 Grenoble, France.

*Corresponding author. E-mail: Mingshang Jin (jinm@mail.xjtu.edu.cn), Kai Chen (kchenlbl@gmail.com).

Experimental Section

Chemicals and materials. Gold (III) chloride hydrate ($HAuCl_4 \cdot 3H_2O$) was obtained from SPC Scientific. Oleylamine (OLA) was obtained from Acros. Copper(II) chloride ($CuCl_2$), copper(II) acetate ($Cu(ac)_2$), trisodium citrate (TSC), sodium borohydride ($NaBH_4$) and potassium iodide (KI) were obtained from Sigma-Aldrich. Gold (III) acetate ($Au(ac)_3$) was obtained from Alfa Aesar. Polyvinylpyrrolidone (PVP, $M_\omega = 10000$) was obtained from Aldrich. L-ascorbic acid (AA) was obtained from Sigma. Acetic acid, ethanol, tetrahydrofuran (THF) and hexane were obtained from Guangdong Guanghua Sci-Tech Co. Ltd. Dimethylphenylsilane, triethylsilane, triphenylsilane, n-propanol and n-butanol were obtained from TCI. Sodium borohydride ($NaBH_4$) and 4-nitrophenol were obtained from China National Pharmaceutical Group Corporation. Commercial carbon (Black EC-300J) was obtained from Ketjen. n-dodecane was obtained from Aladin. All water used in the experiments was deionized water with a resistivity of 18.2 MΩ cm.

Preparation of heterophase Au NWs. In a typical synthesis, 1.25×10^{-2} mmol $HAuCl_4$, 5×10^{-2} mmol $CuCl_2$ and 6 mL OLA was mixed by magnetic and ultrasonic stirring in a 20 mL glass bottle. The aquamarine blue mixture was transferred to an oil bath, which had been heated to 160 ºC, and allowed to react for 4 minutes. After the reaction, the solution turned dark red. The product was collected by centrifugation and washed three times using ethanol/hexane (volume ratio: 5:1).

Preparation of *fcc* Au NWs with high-density planar defects and stepped surfaces. The heterophase Au NWs were treated in acetic acid. The metastable *hcp* phase in the

Au NWs then changed to the *fcc* phase. The acetic acid treatment was carried out according to a protocol reported previously.[1] In detail, the heterophase Au NWs were placed into the same volume of acetic acid. The mixture was transferred to an oil bath and heated at 60 ºC for 3 h. The products were collected by centrifugation and washed with ethanol twice.

Preparation of Au NPs. Au NPs were prepared by a seeded growth method that has been reported previously.[2] In detail, a seed solution was prepared by injecting 0.6 mL of $NaBH_4$ (0.01 M, aqueous solution) into a 43 mL aqueous solution containing 1.16×10^{-4} M $HAuCl_4$ and 5.81×10^{-4} M TSC under vigorous stirring. The solution was stirred for 1 h and remained static for 6 h before use. A growth solution of Au was prepared by incorporating 4.8 mL of 5 wt% PVP, 2.4 mL of 0.2 M KI, 2.4 mL of 0.1 M AA and 0.6 mL of 0.25 M $HAuCl_4$ in 24 mL of H_2O. Seeded growth of Au NPs involved injecting 100 mL of the seed solution into the growth solution under vigorous stirring. After 10 min, Au NPs were centrifuged and washed twice using deionized water.

The equal mass concentration ethanol solution of heterophase Au NWs (catalyst 1), *fcc* Au NWs with high-density planar defects and stepped surfaces (catalyst 2) and Au NPs (catalyst 3) were loaded onto commercial C (15% loading). The use of commercial C as a substrate is intended to ensure dispersion of the Au catalysts for catalytic tests. After loading, the ethanol was removed by washing in equal volume deionized water three times. ICP-MS was used for concentration calibration.

Catalytic silane oxidation reactions. 2 mL of THF was added in a 20 mL hard-glass reactor outfitted with a magneton and a rubber stopper. 0.2 mmol dimethylphenylsilane (purity, >97%) was then introduced into the reactor under ultrasonic mixing. The reactor was mixed for 10 min. Au catalysts (0.1 mol%; the deionized water volume in all experiments was 0.1 mL) were added. After 25 min, the reactor was taken out and cooled in an ice bath to stop the reaction quickly. The product was collected for further analysis. For the TOF calculations, all of the catalytic reaction conversion rates are less than 10%. For the stability test, catalyst 1 was collected from the catalytic reaction by centrifugation and washed using quantitative THF. For GC-MS measurement, a frequently-used reagent, n-dodecane, was selected as an internal standard.

Catalytic 4-nitrophenol reduction reactions. Initially, 5×10^{-2} mmol 4-nitrophenol and 1 mmol% Au catalysts were dispersed into 5 mL water in a 20 mL glass bottle with a magneton. Then, 2 mL freshly prepared 0.5 M $NaBH_4$ solution was added quickly, and the reaction started immediately. The catalytic reduction of 4-nitrophenol was analyzed by UV-vis absorption spectroscopy.

PXRD sample preparation. *First preparation method.* Au NWs were dispersed in 1.5 mL hexane in a centrifugation tube. The colloidal solution was added dropwise onto a clean glass slide. *Second preparation method.* For synchrotron PXRD experiments, Au NWs were dispersed in trace hexane in a centrifugation tube, and the vacuum pump was used to dry the NWs. The dried Au NWs were packed into 0.5-mm-sized borosilicate capillaries and compacted. *Third preparation method.* Au NWs were dispersed in 1.5 mL hexane in a centrifugation tube. The colloidal solution was added dropwise onto a clean glass slide. After the sample had dried, another clean glass slide was used to press the sample for PXRD characterization. *Fourth preparation method.*

This preparation is referred to the synchrotron PXRD specimen preparation method. Typically, Au NWs were dispersed in trace hexane in a centrifugation tube, and the vacuum pump system was used to dry the NWs. The dried Au NWs were packed into 0.5-mm-sized borosilicate capillaries and compacted. The capillaries were broken up (the lab based PXRD equipment cannot obtain the signals when the samples are in the capillary) and the compacted Au NW powder was taken out. The powder was pressed onto a clean glass slide. The four preparation methods are illustrated in Scheme S1.

Characterizations. Transmission electron microscopy (TEM) images were obtained using a Hitachi HT-7700 operated at 100 kV. Basic high-resolution (HR) TEM analyses were carried out using JEM-F200 and Philips Tecnai F20 FEG-TEM microscopes operated at 200 kV. Scanning electron microscopy (SEM) characterization was carried out using a FEI Quanta 250 FEG at 30 kV. PXRD was carried out using a diffractometer (DMAX/A, Rigaku), which was operated at 40 kV with a 30-mA current and Cu K radiation. Elemental analysis was performed using NexION^{TM} 350D, PerkinElmer (PE) inductively coupled plasma mass spectrometry (ICP-MS). Ocean Optics HR2000+ES UV-vis-NIR spectrophotometer with a DH-2000 Bal light source was used for analyses of 4-nitrophenol reduction reactions. Agilent 5970C GC-MS (with a thermal conductivity detector) and Bruker Avance-400 spectrometer nuclear magnetic resonance (NMR) were used for structure analyses of organic reaction conversions and products.

Synchrotron PXRD. High-resolution powder diffraction data were collected at the high-resolution powder diffraction beamline ID22 in the European Synchrotron

Radiation Facility (Grenoble, France). The sample was packed in a 0.5-mm-diameter borosilicate capillary and measured at an energy of 31 keV (0.399924 Å). Four 2θ scans were recorded at a speed of 1°/min over 45° (2θ) and summed. Pawley fits were carried out using TOPAS software (version 5.0, Bruker AXS: Karlsruhe, Germany). Two excluded regions that included parasitic signals were defined between 7° and 8° (2θ) and between 12.7° and 13.7° (2θ). Pawley refinement (R_{wp}=4.3, R_{exp}=3.2, R_{p}=3.2, GOF=1.3) was carried out using two phases in the structural model: Au *fcc* (cubic symmetry, space group Fm3m) and Au *hcp* (hexagonal symmetry). In order to investigate the most probable dimension of the *c* cell parameter of the *hcp* phase, refinements were carried out using space group P6. During refinement, cell parameters of both the *fcc* and the *hcp* phases, peak shape profile parameters and the zero-point parameter were allowed to vary.

High-resolution aberration-corrected electron microscopy. Aberration-corrected electron microscopy was used to analyze the structures of typical Au NWs. High-resolution TEM was performed at 300 kV on an FEI Titan G2 60-300 microscope[3] equipped with a high-brightness field emission gun (X-FEG) and a spherical aberration (C_{S}) corrector for the objective lens. Images were recorded over focus in the negative C_{S} imaging (NCSI) mode, providing bright atom contrast on a dark background. Atomic-resolution high-angle annular dark-field (HAADF) STEM imaging was carried out at 200 kV on a FEI Titan G2 80-200 ChemiSTEM microscope[4] equipped with an X-FEG and a probe C_{S} corrector. The beam semi-convergence angle was 24.7 mrad and the inner detector collection semi-angle was ~70 mrad. All electron microscopy images shown in this paper are raw images without any post-filtering.

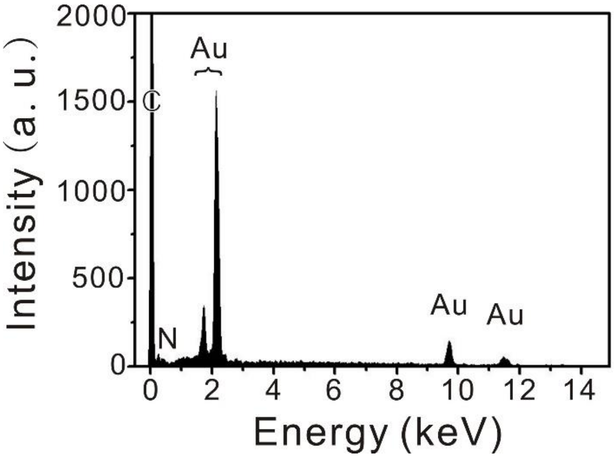

Figure S1. SEM-EDS of Au NWs. The spectrum confirms that the NWs are composed of pure Au, with OLA adsorbed on their surfaces.

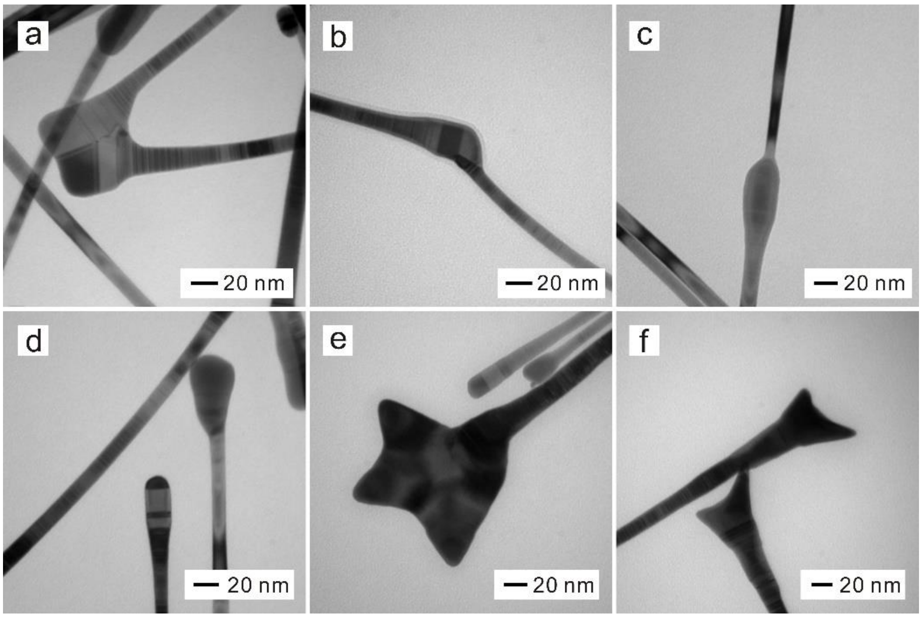

Figure S2. Representative TEM images of Au NWs. The images show typical features of the Au NWs, including swollen segments with different shapes at their ends.

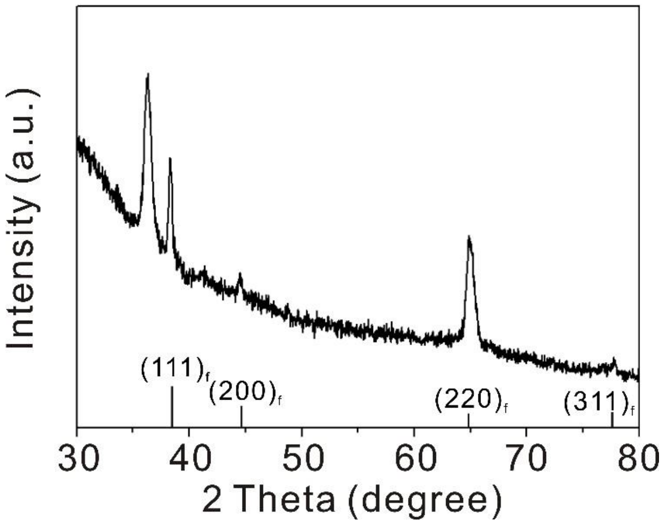

Figure S3. Lab-based PXRD pattern recorded from Au NWs. The sample used in this test was prepared by the first method (see the experimental section). The result shows that Au NWs have mixed *hcp* and *fcc* phases.

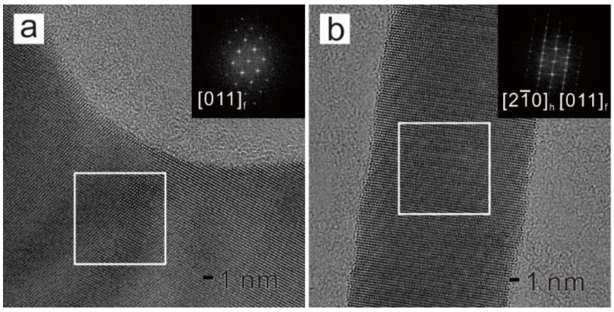

Figure S4. Representative HRTEM images and corresponding FFT patterns of Au NWs. The inset FFT patterns were generated from the white squares in the images. (a) HRTEM image and FFT pattern of swollen region of the Au NWs, showing that a pure *fcc* phase. (b) HRTEM image and FFT pattern of the bodies of Au NWs, showing a mixture of *hcp* and *fcc* phases.

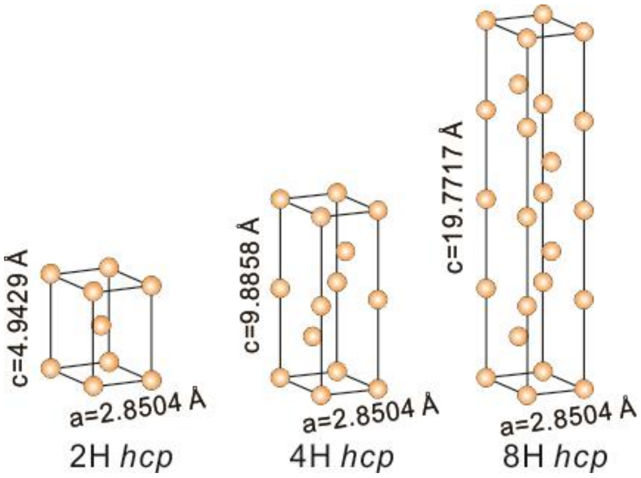

Figure S5. Schemes for 2H, 4H and 8H unit cells. The figure shows unit cells of 2H with *AB* stacking, 4H with *ABCB* stacking and 8H with *ABCBCBAB* stacking, each of which were observed in HRTEM images (Figure 2h-j).

There are significant differences in peak intensity ratio between the lab-based PXRD (first preparation method) and synchrotron PXRD (second preparation method) results (Figure S3 and Figure 4a).

In the lab-based PXRD result (Figure S3), the intensity ratio of the *hcp* peaks (~36.3°[a] and ~40.8°[b]) is far from the ideal model, suggesting that the specimen shows the signally texture.[5] HRTEM characterizations (Figure 2, 3 and Figure S4) show that the *fcc* phase is the major structure in the NWs (the swollen region and parts of the bodies of the NWs adopt the *fcc* phase). Based on the PXRD results (Figure S3 and Figure 4a) and above discussion, we used two more preparation methods to assess the results: the third and fourth preparation methods (experimental section). The resulting PXRD patterns are shown in Supplementary Figure S6 and S7, respectively. The variation in the peak intensity ratios for the different preparation methods suggests that the different peak intensities are associated with textures resulting from the different sample preparation methods.

Comments.

[a] (002) and (010) for 2H, (004) and (010) for 4H, (006) and (010) for 6H, (008) and (010) for 8H.

[b] $(1\bar{1}1)$ and (011) for 2H, $(1\bar{1}2)$ and (012) for 4H, $(1\bar{1}3)$ and (013) for 6H, $(1\bar{1}4)$ and (014) for 8H.

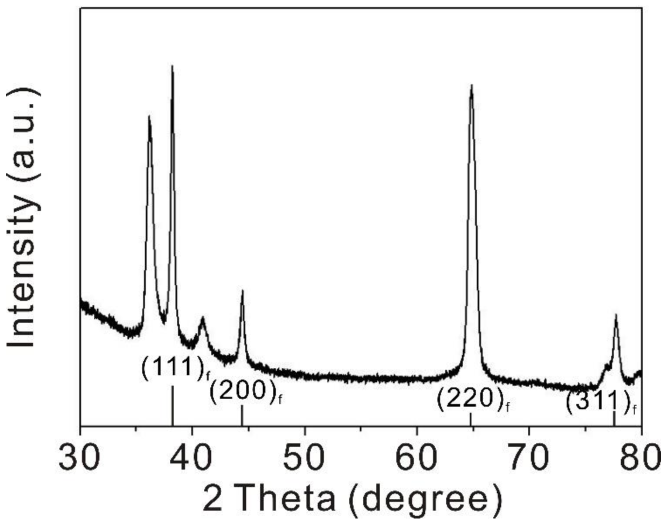

Figure S6 Lab-based PXRD pattern of Au NWs. The sample used in this test was prepared using the third method (see details in the experimental section). In this test, the *hcp*/*fcc* peak intensity ratio is decreasing slightly, when compared with the first preparation method (Figure S3).

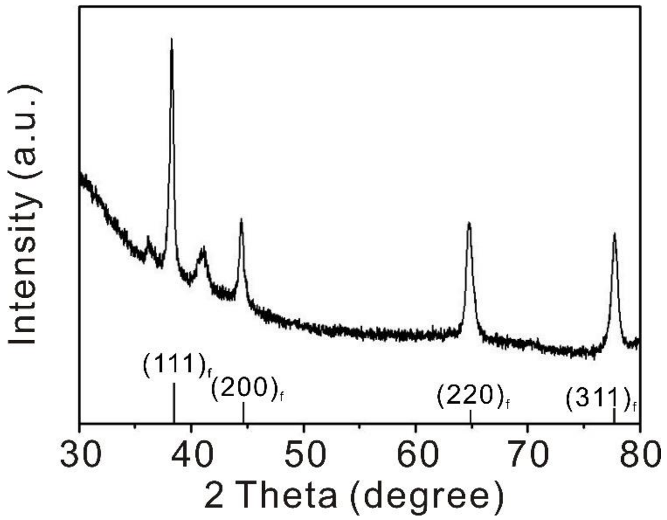

Figure S7. Lab-based PXRD pattern of Au NWs. The sample used in this test was prepared using the fourth method (see details in the experimental section). In this test, the *hcp*/*fcc* peak intensity ratio is apparently decreased, when compared with the first and third preparation methods (Figure S3 and S6), while it exhibits a slight increase when compared with the second preparation method (Figure 4).

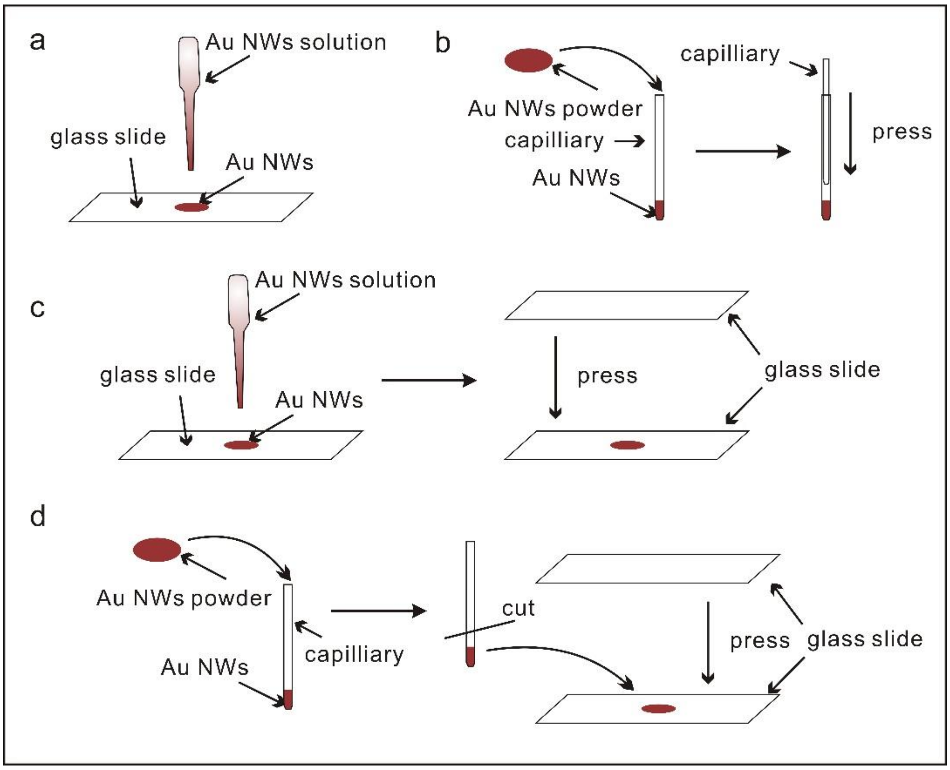

Scheme S1. Four PXRD sample preparation methods. (a) First preparation method. (b) Second preparation method. (c) Third preparation method. (d) Fourth preparation method.

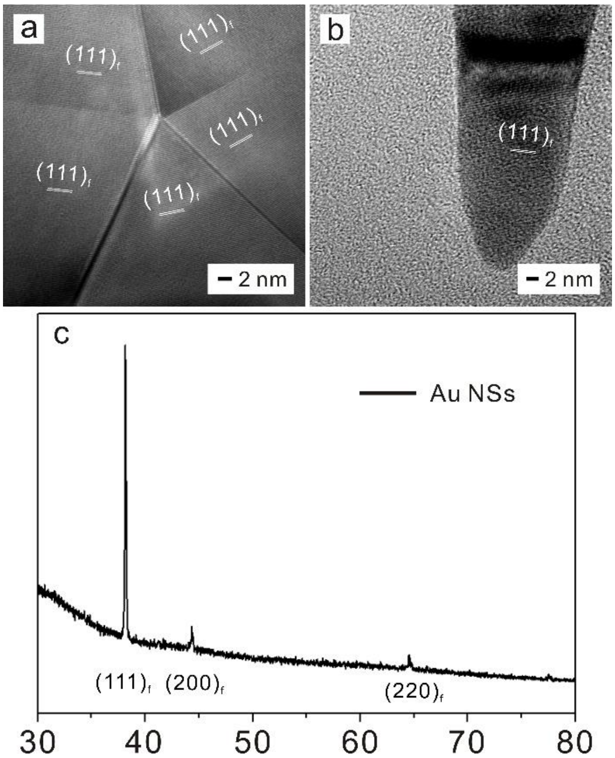

Figure S8. Representative HRTEM images and lab-based PXRD pattern of Au NSs. (a) HRTEM image of the center region of a Au NS. (b) HRTEM image of an angle in a Au NS. (c) Lab-based PXRD pattern of Au NSs (first preparation method). The HRTEM and lab-based PXRD results are consistent with a pure *fcc* structure in Au NSs.

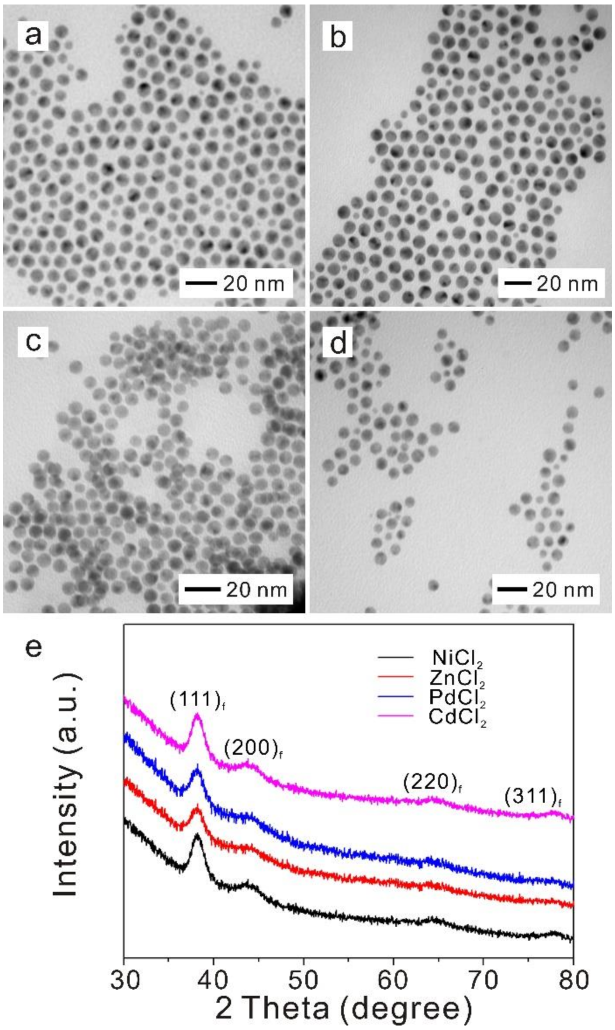

Figure S9. Representative TEM images and lab-based PXRD patterns (first preparation method) of the products. Reaction conditions: equal molar quantity hydrochlorides replaced $CuCl_2$ in the synthesis. (a) $NiCl_2$, (b) $ZnCl_2$, (c) $PdCl_2$, (d) $CdCl_2$. (e) PXRD patterns of the four experimental products. The metal elements in the four hydrochlorides are the nearest and diagonal elements of copper in the periodic table of elements. Only Au NPs in the *fcc* phase are obtained, highlighting the important role of Cu^{2+} in the formation of intermediate penta-twinned Au NSs and final Au NWs.

Experimental conditions: 1.25×10^{-2} mmol of $HAuCl_4$, 5×10^{-2} mmol of MCl_2 (M = Ni, Zn, Pd, Cd), and 6 mL of OLA was mixed by magnetic and ultrasonic stirring in a 20-mL glass bottle. The uniform mixture was transferred to an oil bath, which had been heated to 160 ºC, and allowed to react for 4 minutes. The product was collected by centrifugation and washed three times using ethanol/hexane (volume ratio: 5:1).

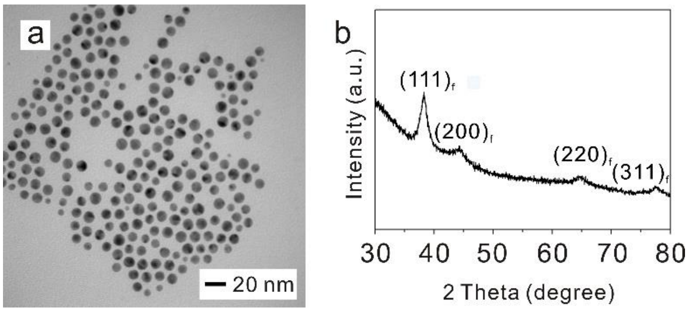

Figure S10. Representative TEM image and lab-based PXRD pattern (first preparation method) of the products. Reaction conditions: CuCl$_2$ free. Only Au NPs in the *fcc* phase are obtained, highlighting the high concentration of Cl$^-$ in the formation of heterophase Au NWs.

Experimental conditions: 1.25×10^{-2} mmol of HAuCl$_4$ was added in 6 mL of OLA by magnetic and ultrasonic stirring in a 20-mL glass bottle. The uniform mixture was transferred to an oil bath, which had been heated to 160 ºC, and allowed to react for 4 minutes. The product was collected by centrifugation and washed three times using ethanol/hexane (volume ratio: 5:1).

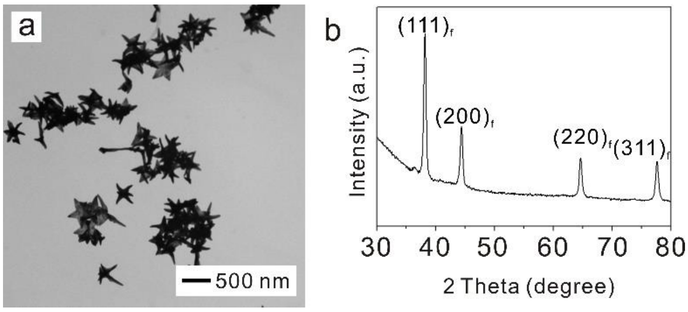

Figure S11. Representative TEM image and lab-based PXRD pattern (first preparation method) of the products. Reaction conditions: equal molar quantities of Cu(ac)$_2$ were used to replace CuCl$_2$ in the synthesis. Only Au NSs in the *fcc* phase are obtained in a low concentration of Cl$^-$ (8.33 mM) reaction mixture, indicating that the formation of heterophase Au NWs requires strong etching.

Experimental conditions: 1.25×10^{-2} mmol of HAuCl$_4$, 5×10^{-2} mmol of Cu(ac)$_2$, and 6 mL of OLA was mixed by magnetic and ultrasonic stirring in a 20-mL glass bottle. The uniform mixture was transferred to an oil bath, which had been heated to 160 ºC, and allowed to react for 4 minutes. The product was collected by centrifugation and washed three times using ethanol/hexane (volume ratio: 5:1).

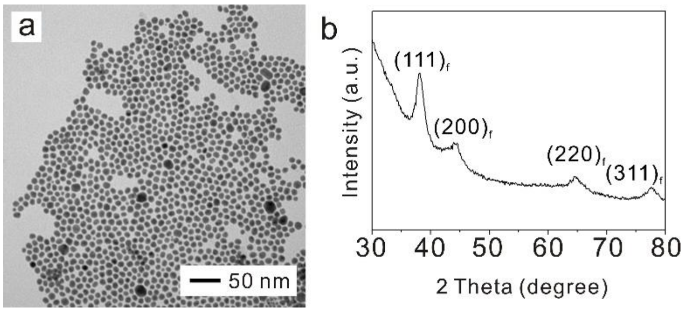

Figure S12 Representative TEM image and lab-based PXRD pattern (first preparation method) of the products. Reaction conditions: equal molar quantities of Au(ac)$_3$ and Cu(ac)$_2$ were used to replace $HAuCl_4$ and $CuCl_2$, respectively, in the standard synthesis. Only Au NPs in the *fcc* phase are obtained in the Cl^--free system, indicating that the formation of heterophase Au NWs requires etching effect.

Experimental conditions: 1.25×10^{-2} mmol of Au(ac)$_3$, 5×10^{-2} mmol of Cu(ac)$_2$, and 6 mL of OLA was mixed by magnetic and ultrasonic stirring in a 20-mL glass bottle. The uniform mixture was transferred to an oil bath, which had been heated to 160 ºC, and allowed to react for 4 minutes. The product was collected by centrifugation and washed three times using ethanol/hexane (volume ratio: 5:1).

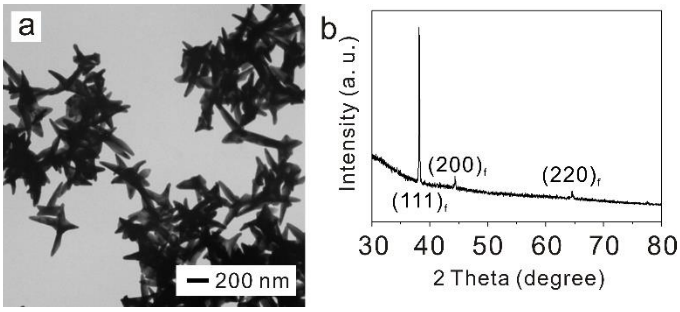

Figure S13. Representative TEM image and lab-based PXRD pattern (first preparation method) of products. Reaction conditions: oxygen-free (injecting nitrogen to remove oxygen; 30 min). The result indicates that the formation of heterophase Au NWs requires strong etching.

Experimental conditions: 1.25×10^{-2} mmol of $HAuCl_4$, 5×10^{-2} mmol of $CuCl_2$, and 6 mL of OLA was mixed by magnetic and ultrasonic stirring in a 20-mL glass bottle. Then, nitrogen was pumped into the uniform mixture for 30 min. After that, the uniform mixture was transferred to an oil bath, which had been heated to 160 ºC, and allowed to react for 4 minutes. The product was collected by centrifugation and washed three times using ethanol/hexane (volume ratio: 5:1).

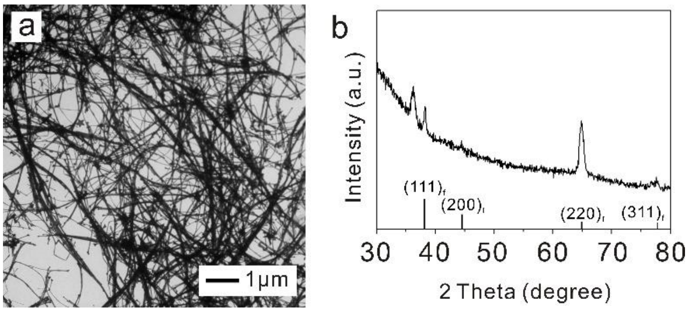

Figure S14. Representative TEM image and lab-based PXRD pattern (first preparation method) of products. Reaction conditions: equal molar quantities of $Au(ac)_3$ were used to replace $HAuCl_4$. The result indicates that the use of a slightly reduced Cl^- concentration (16.7 mM) does not affect the formation of the heterophase Au NWs. Experimental conditions: 1.25×10^{-2} mmol of $Au(ac)_3$, 5×10^{-2} mmol of $CuCl_2$, and 6 mL of OLA was mixed by magnetic and ultrasonic stirring in a 20-mL glass bottle. The uniform mixture was transferred to an oil bath, which had been heated to 160 ºC, and allowed to react for 4 minutes. The product was collected by centrifugation and washed three times using ethanol/hexane (volume ratio: 5:1).

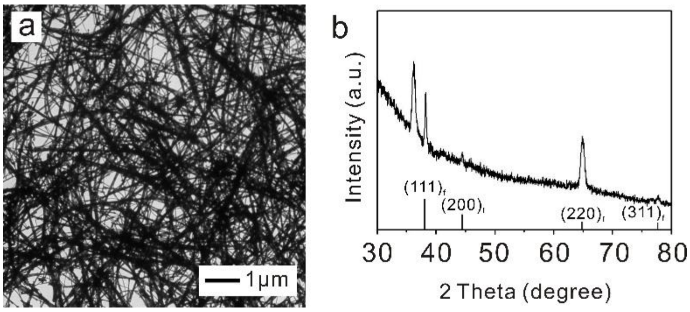

Figure S15. Representative TEM image and lab-based PXRD pattern (first preparation method) of products. Reaction conditions: equal molar quantities of Cu(ac)$_2$ were used to replace CuCl$_2$ and added the equal molar quantities NiCl$_2$. The result indicates that heterophase Au NWs can be synthesized successfully when using other hydrochloride to supply the shortage of Cl$^-$.

Experimental conditions: 1.25×10^{-2} mmol of HAuCl$_4$, 5×10^{-2} mmol of Cu(ac)$_2$, 5×10^{-2} mmol of NiCl$_2$, and 6 mL of OLA was mixed by magnetic and ultrasonic stirring in a 20-mL glass bottle. The uniform mixture was transferred to an oil bath, which had been heated to 160 ºC, and allowed to react for 4 minutes. The product was collected by centrifugation and washed three times using ethanol/hexane (volume ratio: 5:1).

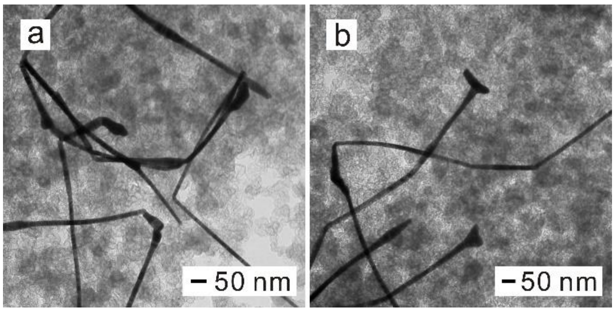

Figure S16. Representative TEM images of Au NWs catalysts. (a) Catalyst 1. (b) Catalyst 2. The results elucidate that the Au NWs have good dispersion after loading on commercial C.

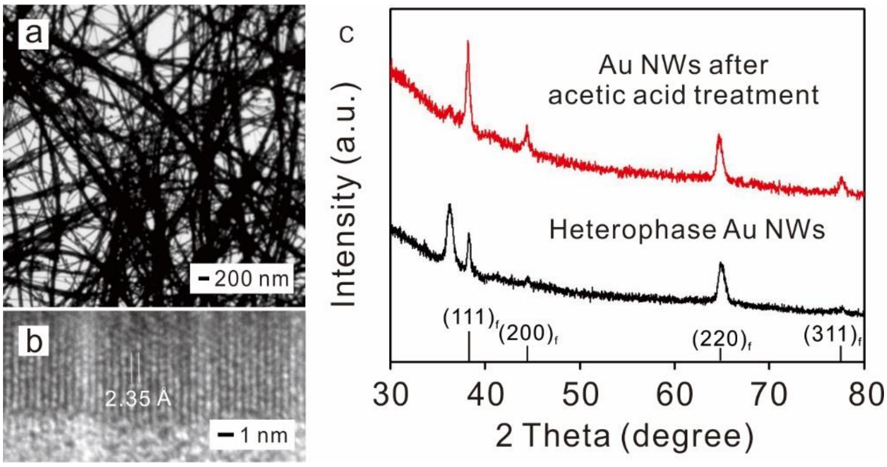

Figure S17. Representative TEM, HRTEM, and lab-based PXRD characterization of Au NWs after acetic acid treatment. (a) TEM image of Au NWs after acetic acid disposal. (b) HRTEM image of Au NWs after acetic acid disposal. Parallel $(111)_f$ crystal facets are visible. Stepped surfaces can be observed in the image. (c) PXRD patterns of heterophase Au NWs and acetic acid disposed Au NWs are shown using black and red lines, respectively (first preparation method; the parallel black lines mark crystal peaks for Au in the *fcc* phase). The results show that nearly all of the metastable *hcp* phases changed to *fcc* structures, with a $[111]_f$ growth direction, under acetic acid treatment.

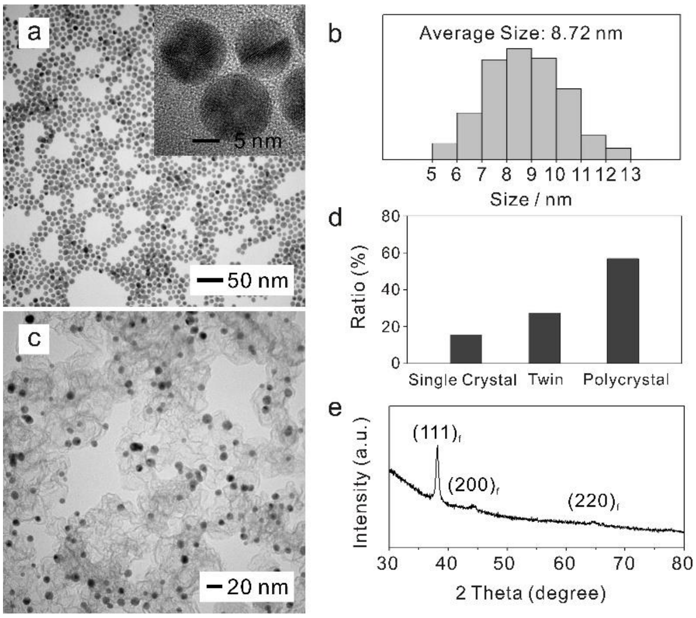

Figure S18. Representative TEM images and lab-based PXRD characterization (first preparation method) of Au NPs (catalyst 3). (a) TEM image. Inset: HRTEM image of Au NPs. (b) Size distribution of Au NPs. (c) Au NPs on commercial C (catalyst 3). (d) The crystalline statistics of Au NPs. (e) PXRD pattern. The results demonstrate that Au NPs in the *fcc* phase with abundant planar-defect surface terminations and average size of 8.72 nm have good dispersion on commercial C.

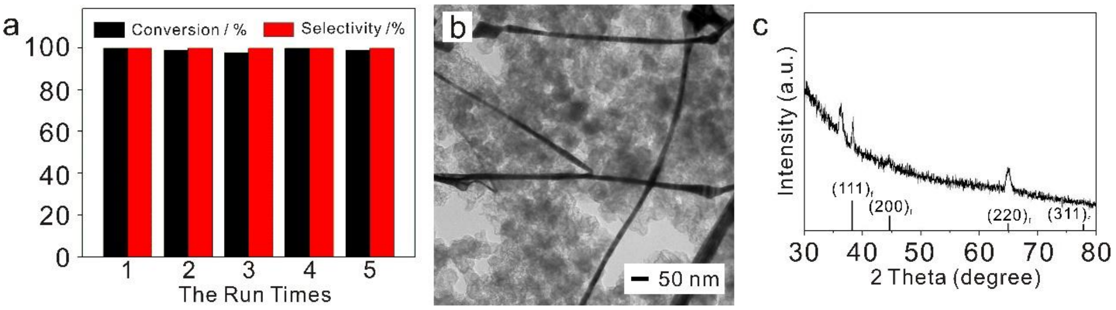

Figure S19. Reusability tests of catalyst 1. Reactants: dimethylphenylsilane and H_2O. (a) Conversion and selectivity of reusable experiments. (b) TEM image of catalyst 1 after being used five times. (c) Lab-based PXRD pattern of catalyst 1 (without carbon loading) after being used five times in a catalytic reaction (first preparation method). The results illustrate the fact that catalyst 1 has good stability and selectivity for silane oxidation.

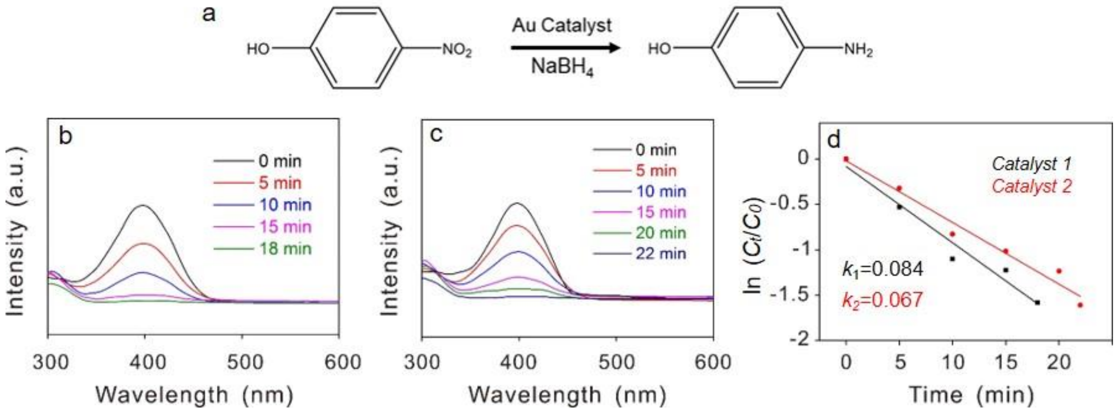

Figure S20. Time-dependent UV-vis spectra of the reaction solution in the presence of the Au catalysts. (a) Equation for the catalytic reduction of 4-nitrophenol to 4-aminophenol. (b) Time-dependent UV–vis spectra of the reaction solution in the presence of heterophase Au NWs (catalyst 1). (c) Time-dependent UV–vis spectra of the reaction solution in the presence of *fcc* Au NWs (catalyst 2). (d) Plot of ln(C_t/C_0) against the reaction time, where *k* is the coefficient of determination obtained from the linear fitting.

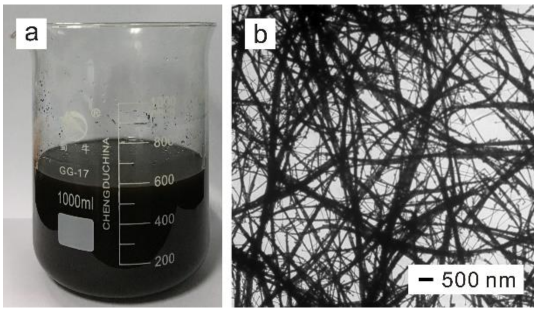

Figure S21. Preparation of Au NWs on a large scale. (a) Magnification of the reaction system by 100 times. (b) Typical TEM image of Au NWs obtained from large-scale preparation.

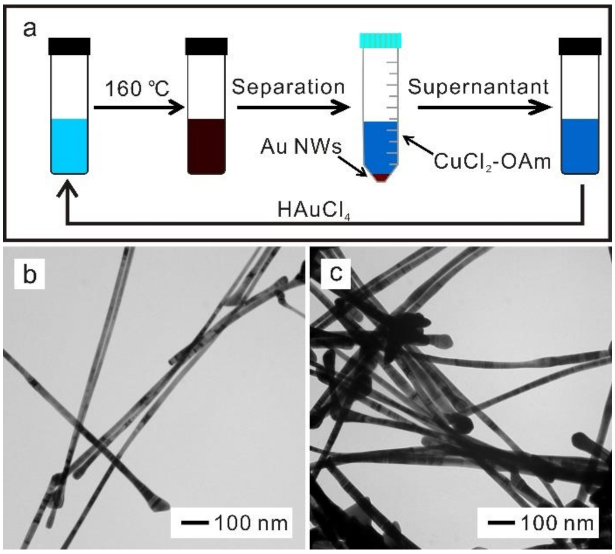

Figure S22. Reaction mixture reusability test results. (a)Experimental scheme. (b, c) TEM images of products with the reaction mixture reused, for the first and second cycles, respectively. The reaction times are prolonged to 5 and 6.5 minutes in the two experiments, respectively. Figure S21 and S22 illustrate the commercial viability of the synthetis approach proposed in this work.

Table S1. Statistics of planar defect density in heterophase Au NWs (catalyst 1) and Au NWs after acetic acid treatment (catalyst 2). The average planar defect density was calculated by dividing the sum of the planar defects by the sum of the NW length. Stacking faults, twin boundaries and phase boundaries are all regarded as planar defects.

Samples	**Treatment**	**Defect density (per 10 nm)**
1	**-**	4.35
2	Acetic acid	4.25

Table S2. Mechanism study of the growth process: Influence of the reactants on the morphology and phase of the final products.

Entry	**Precursor**	**Cu^{2+}**	**Cl^- (mM)**	**Oxygen**	**Phase**	**Schematic drawing**
1[a]	$HAuCl_4$	+	25	✓	*fcc/hcp*	
2[b]	$HAuCl_4$	-	8.33	✓	*fcc*	
3[c]	$HAuCl_4$	+	8.33	✓	*fcc*	
4[d]	$Au(Ac)_3$	+	0	✓	*fcc*	
5[e]	$HAuCl_4$	+	25	-	*fcc*	
6[f]	$Au(Ac)_3$	+	16.67	✓	*fcc/hcp*	
7[g]	$HAuCl_4$	+	25	✓	*fcc/hcp*	

All the experiments use OLA as the solvents. [a] Typical reaction conditions. [b-g] The experimental results are shown in the supporting information, Figure S10-Figure S15, respectively.

Table S3 Au-catalyst-catalyzed oxidation of different substrates.

$$R(R')_2SiH + R''OH \xrightarrow[\text{THF, air}]{\text{Au Catalysts}} R(R')_2SiOR'' + H_2$$

Entry	Silane	Hydroxy-containing	Temperature (°C)	Time (min)	Yield (%)
1[a]	$Ph(Me)_2SiH$	H_2O	25	25	>99
2[b]	$Ph(Me)_2SiH$	H_2O	25	25	50.6
3[c]	$Ph(Me)_2SiH$	H_2O	25	25	11.2
4[a]	$Ph(Me)_2SiH$	EtOH	25	30	>99
5[a]	$Ph(Me)_2SiH$	*n*-PrOH	25	30	>99
6[a]	$Ph(Me)_2SiH$	*n*-BuOH	25	30	>99
7[a]	$(Et)_3SiH$	H_2O	25	60	>98
8[a]	$(Ph)_3SiH$	H_2O	50	90	>99

a. Catalyst 1. b. Catalyst 2. c. Catalyst 3. Reaction conditions: Entries 1-3, 7, and 8 are 0.2 mmol silanes, 100 µL H_2O, and 0.1 mmol% Au catalysts, and 2 mL tetrahydrofuran (THF). Entries 4-6 are 0.2 mmol silanes, 0.1 mmol% Au catalysts, and 2 mL corresponding alcohols.

Table S4 Comparison of typical heterogeneous Au catalytic systems for the oxidation of dimethylphenylsilane with water.

Entry	Catalyst	Temperature (°C)	Time (h)	TON
1[a]	Catalyst 1	25	1	63640
2	KCC-1-APTS/Au[6]	45	22	591000
3	Nanoporous Au[7]	25	1	10700
4	Au/CNT[8]	25	6	72000
5	Au/CNT[9]	25	12	61000

a. Reaction conditions: 2.5 mmol dimethylphenylsilane, 0.02 mol% Catalyst 1, 4 mL H_2O.

Reference.

(1) Li, X. Chen, Q.; Wang, M.; Cao, Z.; Zhan, Q.; He, T.; Kuang, Q.; Yin, Y.; Jin, M. *J. Mater. Chem. A* **2016**, *4*, 13033-13039.

(2) Ding, D.; Liu, K.; He, S.; Gao, C.; Yin, Y. *Nano Lett.* **2014**, *14*, 6731-6736.

(3) Boothroyd, C.; Kovács, A.; Tillmann, K. *Journal of large-scale research facilities* **2016**, *2*, A44.

(4) Kovács, A.; Schierholz, R.; Tillmann, K. *Journal of large-scale research facilities* **2016**, *2*, A43.

(5) Wang, C.; Daimon, H.; Lee, Y.; Kim, J.; Sun, S. *J. Am. Chem. Soc.* **2007**, *129*, 6974-6975.

(6) Dhiman, M.; Chalke, B.; Polshettiwar, V. *J. Mater. Chem. A* **2017**, 5, 1935-1940.

(7) Asao, N.; Ishikawa, Y.; Hatakeyama, N.; Menggenbateer; Yamamoto, Y.; Chen, M.; Zhang, W.; Inoue, A. Angew. Chem. Int. Ed. 2010, 49, 10093-10095.

(8) John, J.; Gravel, E.; Hagège, A.; Li, H.; Gacoin, T.; Doris, E. Angew. Chem. Int. Ed. 2011, 50, 7533-7536.

(9) Liu, T. Yang, F.; Li, Y.; Ren, L.; Zhang, L.; Xu, K.; Wang, X.; Xu, C.; Gao, J. J. Mater. Chem. A 2014, 2, 245-250.